
LIGHTWEIGHT SOFTWARE KERNELS AND HARDWARE EXTENSIONS FOR EFFICIENT SPARSE DEEP NEURAL NETWORKS ON MICROCONTROLLERS

Francesco Daghero¹ Daniele Jahier Pagliari¹ Francesco Conti² Luca Benini^{2,3} Massimo Poncino¹
Alessio Burrello¹

ABSTRACT

The acceleration of pruned Deep Neural Networks (DNNs) on edge devices such as Microcontrollers (MCUs) is a challenging task, given the tight area- and power-constraints of these devices. In this work, we propose a three-fold contribution to address this problem. First, we design a set of optimized software kernels for N:M pruned layers, targeting ultra-low-power, multicore RISC-V MCUs, which are up to $2.1\times$ and $3.4\times$ faster than their dense counterparts at 1:8 and 1:16 sparsity, respectively. Then, we implement a lightweight Instruction-Set Architecture (ISA) extension to accelerate the indirect load and non-zero indices decompression operations required by our kernels, obtaining up to $1.9\times$ extra speedup, at the cost of a 5% area overhead. Lastly, we extend an open-source DNN compiler to utilize our sparse kernels for complete networks, showing speedups of $3.21\times$ and $1.81\times$ on a ResNet18 and a Vision Transformer (ViT), with less than 1.5% accuracy drop compared to a dense baseline.

1 INTRODUCTION

The execution of Deep Neural Networks (DNNs) on extreme edge devices, such as IoT end-nodes based on Microcontrollers (MCUs), has become increasingly popular (Wang et al., 2020). Local execution enables smart capabilities in these devices while avoiding the costly transmission of raw data, with advantages in latency predictability, data privacy, and energy efficiency (Sze et al., 2017; Shi et al., 2016). However, since edge devices operate on tight memory and power constraints, DNNs need to be extensively optimized before they can be deployed on MCUs. Techniques such as neural architecture search (Wu et al., 2019), quantization (Wu et al., 2020; Nagel et al., 2021), and pruning (Yu et al., 2017; Trommer et al., 2021) aim at reducing DNNs’ memory occupation and computational requirements while limiting accuracy drops.

In particular, weight pruning removes (i.e., sets to zero) the least relevant weights of a DNN, with potential benefits for both memory and computation, as operations involving zeroed-out weights can be skipped (Yu et al., 2017). However, sparse workloads have less regular memory accesses and lower arithmetic intensity than their dense counterparts, leading to lower-than-expected performance gains when leveraging HW/SW stacks not explicitly designed for sparsity, especially at low pruning ratios (Yu et al., 2017). In the State-of-the-Art (SotA), this issue is tack-

led by a combination of model-, software- and hardware-level countermeasures. At the DNN model level, *structured* or *semi-structured* pruning forces specific patterns in the positions of non-zero (NZ) weights, simplifying memory access and indices storage. A popular example is N:M pruning, in which exactly N weights are NZ, in every group of M (Zhou et al., 2021). Several solutions for accelerating sparse workloads have been proposed at lower levels of the stack, ranging from optimized software kernels to custom hardware. The latter includes complete accelerators (Chen et al., 2019; Peltekis et al., 2024), functional units within a CPU pipeline (Jeong et al., 2023), or tensor core extensions, such as the one featured by the NVIDIA A100 GPU family (NVIDIA, 2024).

Extending sparsity support to MCUs, however, is not trivial, as their tight area and power constraints often do not allow the additional overhead of a complete accelerator or complex core modifications. The few existing works (Scheffler et al., 2023) target unstructured sparsity, not exploiting the advantages of constrained pruning patterns such as N:M. As a consequence, they require the availability of uncommon HW features, such as Streaming Semantic Registers (SSRs), which contribute significantly to the total area of the system. At the same time, purely software solutions are complex to implement on MCUs, which feature simple ISAs with limited vectorial capabilities.

This work tries to overcome this gap by proposing a solution for the acceleration of semi-structured N:M sparsity on MCUs. Specifically, our contributions are the following:

¹Politecnico di Torino, Turin, Italy ²University of Bologna, Bologna, Italy ³ETH Zurich, Zurich, Switzerland.

- We design a set of software kernels for 1:4, 1:8, and 1:16 sparsity on MCUs, targeting both convolutions (Conv) and fully-connected (FC) layers. With software only, we achieve speedups ranging from $1.1\times$ to $1.85\times$ for Conv and from $1.02\times$ to $3.4\times$ for FC with respect to the best dense library available, on the RISC-V MCU presented in (Rossi et al., 2021), featuring an 8-core Parallel-Ultra-Low-Power (PULP) cluster.
- We then extend the ISA of our target with a new, *lightweight* instruction, aimed at improving the efficacy of our sparse kernels. Specifically, we accelerate the *activations decimation* (i.e., the selection of activations corresponding to NZ weights), enabling efficient use of the available Single Instruction Multiple Data (SIMD) instructions. Implementing this extension incurs an area overhead of 5.0%, but allows our kernels’ to obtain up to $1.9\times$ extra speedup.
- Lastly, we instrument a DNN compiler (Hamdi et al., 2024) to use our sparse kernels. On two complete DNNs, a Convolutional Neural Network (CNN) and a Vision Transformer (ViT), we achieve a latency reduction of $1.31\times$ and $1.43\times$, respectively, using 1:4 sparsity, with no accuracy loss. At 1:16 sparsity, with an accuracy drop $<1.5\%$, we show speedups of $3.21\times$ for the CNN and $1.81\times$ for the ViT.

2 BACKGROUND

2.1 DNN Pruning

Several works have shown how large portions of weights can be pruned with limited impact on the prediction quality of DNNs (Ma et al., 2023; Park et al., 2016). Optimized implementations of pruned models leverage compressed representations for the sparse weights matrices, storing only NZ elements and the corresponding coordinates. Only the activations corresponding to NZ weights are loaded and processed at inference time, while computations associated with zeroed weights are skipped.

Our work focuses on optimizing the execution of an already pruned DNN. Therefore, it is orthogonal to the specific pruning *strategy*, i.e., the method used to select what and when to prune (for example, using weights magnitude or 1st/2nd order loss approximations). We refer readers to (Hoefler et al., 2021) for a comprehensive survey on this topic. In the rest of this section, we focus instead on the most common pruning *patterns* (i.e., constraints on the position of NZ weights to improve sparse layers’ efficiency); then, we detail common data structures for sparse tensors.

Pruning Patterns: Fig. 1 depicts three common pruning patterns proposed in the literature. *Unstructured* (i.e., unconstrained) pruning leads to the highest compression ratio for a

given accuracy target. However, accelerating unconstrained sparse workloads is challenging: skipping computations requires performing multiple indirect memory loads with an irregular pattern, significantly impacting arithmetic density, as well as cache/scratchpad hit rates. Therefore, for non-extreme sparsity ratios, layers with unstructured sparsity are often even slower than their dense counterparts (Yu et al., 2017).

Structured pruning introduces constraints on the location of the NZ elements, yielding more regular data, at the cost of lower accuracy for the same sparsity (Li et al., 2022b; Tan et al., 2022; Guo et al., 2020). For instance, *block-wise sparsity* (Li et al., 2022b) preserves dense groups of NZ elements of dimension $A \times B$ to increase L1 memory and register utilization, but forcing such coarse-grained patterns usually yields large accuracy drops (Li et al., 2022b). Extremizing this concept, *feature* or *channel* pruning (Li et al., 2022a), not shown in the figure, eliminates entire *rows* of the weight matrix, producing a result that is equivalent to a dense (but smaller) weight tensor, thus removing all the difficulties of sparsity, but worsening performance even more.

The N:M approach represents a middle-ground between unstructured and block-wise sparsity (often referred to as *semi-structured*), enforcing the constraint of N non-zero elements in every group of M values. This scheme facilitates load balancing and parallelism at all levels (multicore, SIMD, etc), as equally-sized tensor portions comprising a multiple of M elements always require the same amount of computation, while also ensuring a partial locality in activation accesses. NVIDIA GPUs have added hardware support for this format starting from the A100 series (NVIDIA, 2020), although limited to 2:4 or 1:2 patterns, depending on the data type.

Sparse Data Structures: Several formats have been introduced in the literature to store the NZ elements of a sparse tensor and the corresponding indices with different memory versus decoding overhead tradeoffs. The simplest COOrdinates (COO) format stores a sparse matrix as three arrays, containing the NZ elements and their (row, column) position. While not requiring any extra computation to obtain the coordinates, this format has a non-negligible memory overhead: using 8-bit integer values and 16-bit indices, the minimum sparsity required to balance the memory overhead is 75%. The Compressed Sparse Rows (CSR) format also uses three one-dimensional arrays containing the NZ elements, the number of elements per row, and the column indices. In practice, CSR compresses the row indexes of the COO format, trading off speed for memory efficiency. However, its memory overhead is still non-negligible, requiring more than 50% sparsity to be advantageous on 8-bit quantized values.

The N:M format, shown in the center of Figure 1, stores

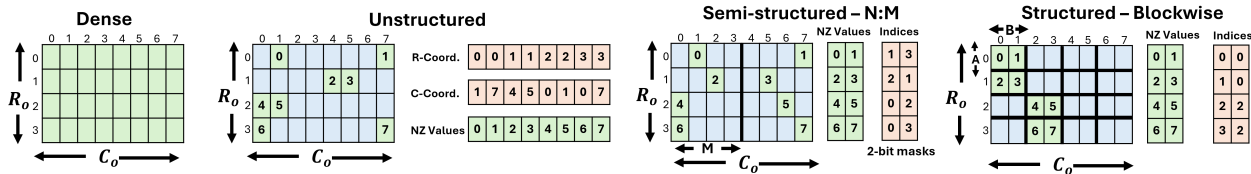


Figure 1. Pruning patterns and indices compressions with 75% sparsity.

sparse data in two matrices. The first contains the NZ values and has dimensions $(R_0, \frac{C_0}{M})$. The second stores the relative indices of the NZ elements within each M -sized block, compressed in $\lceil \log_2(M) \rceil$ bits, usually rounded to the nearest larger power-of-two (e.g., $M=8$ uses 4 bits). This format enables memory-efficient storage even at low sparsity ratios, such as 1:2, but requires additional unpacking operations to extract the compressed indices.

2.2 IoT Edge Nodes

The compute platforms in IoT edge nodes are traditionally centered around low-power and low-cost MCUs. However, in recent years, these devices have been progressively equipped with more advanced features to support the efficient local execution of advanced applications such as Digital Signal Processing (DSP) and DNNs. Accordingly, it is not uncommon for modern MCUs to include multiple processing elements and specialized instructions such as SIMD. At the same time, since energy and area costs remain critical, these devices often give up cache memories in exchange for a multi-level hierarchy of software-controlled scratchpads, where data transfers between levels are handled through Direct Memory Access (DMA) controllers. Companies like STM (STMicroelectronics, 2024), NXP (NXP, 2024) and GreenWaves (GreenWaves, 2024) have already commercialized such architectures.

In this work, we target the Vega PULP SoC (Rossi et al., 2021), which features 10 RISC-V cores and is the blueprint architecture for commercial products such as GreenWaves’ GAP9 (GreenWaves, 2024). In Vega, one core acts as the Fabric Controller (FC), managing peripherals and orchestrating the entire workload; one controls the DMA set-up; the other 8 are organized as a cluster to speed up computation. All cores feature an extended ISA including SIMD dot product instructions on 8-bit integers, loads with automatic post increment, and hardware loops to accelerate DSP and DNN workloads. The SoC features a 128 kB L1 data memory, shared between all cluster cores, a 1.6 MB L2 main memory (comprising an MRAM memory, which we do not exploit), and 16 MB of external L3 HyperRAM memory.

3 RELATED WORKS

Many works in the literature have focused on accelerating sparse DNN workloads. Some of them target high-end CPUs/GPUs, either introducing novel software kernels to exploit existing HW or proposing HW extensions to achieve higher speed-ups. For instance, the authors of (Wang, 2021; Castro et al., 2023; Jeong et al., 2023) exploit graph-level optimizations, custom sparsity formats and new instructions to achieve speedups of up to 4x w.r.t. dense baselines. Other works design complete HW accelerators, achieving impressive speed-ups at the cost of significant area overheads (Chen et al., 2019; Peltekis et al., 2024; Han et al., 2016).

While less explored, some articles also target the execution of sparse DNNs on MCUs. In (Yu et al., 2017), the authors propose pruning groups of weights with the same dimension as the target’s SIMD width, so that, at inference time, SIMD instructions can still be utilized. This is a particular instance of blockwise pruning with dimensions $A \times B = 1 \times \text{SIMD-width}$. They benchmark their custom kernels on an ARM Cortex M4 MCU with 2-way fixed-point SIMD instructions, obtaining maximum speedups of $1.38 \times$ on a ConvNet at 59.95% sparsity and of $3.51 \times$ on a LeNet-5 at 93.28% sparsity, among CNNs. Additionally, they achieve a speed-up of $9.17 \times$ at 93.07% sparsity on a LeNet300, composed only of FC layers. However, on the tested MCU, weights are directly loaded from Flash memory, with high latency. Therefore, the benefits of skipped loads due to SIMD-aware pruning hide the overheads of blockwise sparse processing, “idealizing” the speedups (absolute inference times would remain very high and bottlenecked by memory accesses). Moreover, as mentioned in Sec. 2, blockwise sparsity can lead to large accuracy drops on more complex DNNs and datasets (Li et al., 2022b) (LeNet is tested on MNIST, while ConvNet reaches 81.86% accuracy on CIFAR10).

The work of (Trommer et al., 2021) focuses on unstructured sparsity, proposing a linear encoding for CSR indices to reduce their memory overhead in exchange for extra decoding operations. They benchmark their approach on an ARM Cortex-M55, using three DS-CNN variants and comparing with two dense baselines derived from CMSIS-NN (Lai et al., 2018), as well as with the storage of relative indices

(RI) in CSR. They achieve a maximum reduction of cycles on the largest DS-CNN of 41.7% compared to the original CMSIS-NN library and 6.7% compared to hand-optimized kernels, with 90% weights sparsity on point-wise Convolutions, and FC layers. They also show a $5.21\times$ memory reduction on the pruned layers, with a memory footprint only 3.5% higher than the CSR’s RI storage. Speedups compared to optimized dense kernels are relatively low due to the large decoding overhead.

The authors of (Titopoulos et al., 2023) implement an ISA extension to accelerate N:M sparsity on a 64-bit RISC-V core paired with a 16-lane 512-bit vector engine. Their new instruction, called IndexMAC, allows low-cost indirect access to row portions of the dense activation matrix, pre-loaded in a vector register file. Moreover, they introduce a set of optimized kernels performing row-wise matrix multiplication with this instruction, achieving $1.82\times/2.14\times/1.92\times$ speed-ups over a SW-only sparse baseline on ResNet50, Densenet121, and InceptionV3 at 75% sparsity. Differently from our work, the deployment target is a high-end RISC-V core, leading to significantly different design choices. First, MCUs do not include a dedicated vector register file and have limited options for data pre-loading, given their small L1 memory size. Second, in their work, NZ indices are stored uncompressed, limiting the memory reduction in exchange for increased throughput. Finally, their vector engine supports 32-bit element vectors and scalar-by-vector operations, while we target 8-bit integer SIMD without any scalar-by-vector instruction.

In (Scheffler et al., 2023), the authors introduce a RISC-V ISA extension to accelerate computations with unstructured sparsity, supporting both CSR and Compressed Sparse Fiber (CSF) formats. They extend RI5CY cores with Sparse Stream Semantic Registers (SSSRs), which transparently load/store data based on a stream of indices, making them available to other instructions (e.g., dot products). This increases FPU utilization by getting rid of explicit load/store instructions. While extremely effective (5x speedup at 95.7% sparsity on GEMMs), SSSRs are targeted for floating point kernels and are not easily extensible to support low-precision integer SIMD calculations. Moreover, SSSRs are complex circuits whose area overhead (≈ 20 to 31 kGE depending on the configuration) is already significant (20-31%) when considering an FPU-equipped RI5CY with its 102 kGE (Schuiki et al., 2020), as baseline. When compared to an FPU-less RI5CY, the overhead increases to as much as 44%. Lastly, CSR and CSF formats require the storage of NZ indices at high precision, thus resulting in significantly higher memory overheads w.r.t. the N:M format.

Table 1. Layer dimensions notation

Tensors	Dimensions	Abbreviations
Input (I)	rows, columns, channels	IX/IY/IC
Output (O)	rows, columns, channels	OX/OY/OK
Weights (W)	filter height/width, channels in/out	FX/FY/CK/K
Activations	Padding/Stride	P/S

4 LIGHTWEIGHT KERNELS FOR N:M SPARSE DNNs ON MCUS

This section describes our sparse convolutional (Sec 4.1) and FC (Sec. 4.2) kernels, focusing first on SW-only versions and then showing how those can be enhanced with a lightweight ISA extension. We detail the HW that implements our new instruction in Sec. 4.3. Our kernels operate on 8-bit data, already stored in L1 memory. To execute full networks, we integrate them in the DNN compiler of (Hamdi et al., 2024), as described in Sec. 4.4. We focus on semi-structured N:M sparsity, given the demonstrated benefits over an unstructured approach with a limited loss in accuracy (Zhou et al., 2021). Namely, we support 1:4, 1:8, and 1:16 formats, as increasing sparsity further would lead to a too high accuracy loss, while reducing it would not lead to any latency benefit. While we target the SoC of (Rossi et al., 2021), our SW-only kernels are general enough to be used on all MCUs from the PULP family, i.e., RISC-V-based multi-core MCUs with hierarchical scratchpad memories (Gautschi et al., 2017), and are written in plain C code. Table 1 reports the notation used in the rest of the paper for layer hyper-parameters.

In all our kernels, we use the format shown in Fig. 1 and detailed in Sec. 2 to store N:M sparse weights. Namely, only NZ weights are stored, together with their indices within the corresponding M-sized block, compressed on 4-bits (for 1:8 and 1:16 sparsity) or 2-bits (for 1:4). Thus, 1:4 sparsity leads to a weight memory reduction of 68.75%, 1:8 of 81.25%, and 1:16 of 90.62% (with int8 weights). Notice that, in the same conditions, the CSR format requires storing K row pointers and $\frac{K \times FX \times FY \times C}{M}$ column indices with a minimum precision of 16-bit (for reasonably sized layers), leading to less than 25% compression at 75% sparsity (i.e., the equivalent of the 1:4 format).

4.1 Convolutional Kernel Library

4.1.1 Dense Baseline

The dense 8-bit kernels utilized as a baseline in our work are taken from the SotA PULP-NN library, described in (Garofalo et al., 2020). Fig. 2 visualizes their internal loop: after performing a partial im2col transformation that reorganizes 2 spatially contiguous input patches into 1-dimensional arrays, the kernel loads the weights of 4 convolutional filters

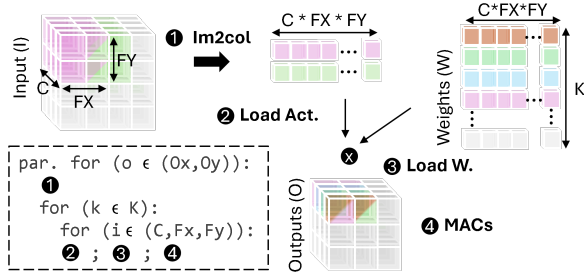


Figure 2. Inner loop of the PULP-NN dense convolutional kernel.

and iterates to produce a total of 8 outputs, (2 different spatial positions, and 4 output channels). The dataflow is output-stationary; all output channels relative to the same spatial positions are produced before moving to the next ones. The detailed loop order is shown in the bottom-left of the figure. The outermost loops over OX and OY are parallelized on the platform’s cores. Furthermore, the MACs of the innermost loop are performed using 4x8-bit SIMD dot product instructions available in the RISC-V XpulpV2 ISA extension (Gautschi et al., 2017). Notice that the partial im2col operation leads to an additional L1 memory requirement of $FX \times FY \times C \times 2 \times N_CORES$ elements.

This kernel achieves a theoretical peak performance in the innermost loop of 2.28 8-bit MACs/instruction/core (32 MACs with 14 instructions, i.e., six load words and 8 SIMD dot-products). However, it cannot be directly extended for sparse layers, as the inner loop unrolling assumes that the input activations used to generate all 4 output channels are identical, which enables reusing the im2col buffers. This is no longer true for N:M sparse layers. Therefore, given the impossibility of implementing such unrolling for sparse kernels, we also consider a dense variant with 1x2 unrolling, i.e., computing a single output channel per internal loop iteration, that reaches a lower theoretical peak of 1.6 MACs/instruction/core. The internal loop of this variant is shown on the left of Fig. 4.

4.1.2 Software-only Sparse Kernel

The SW-only versions of our sparse kernels only exploit instructions from the XpulpV2 extension, already available in (Rossi et al., 2021). They have the same data flow and data stationarity of the dense baseline and use an innermost loop unrolling factor of 1x2, i.e., over two consecutive input patches and one weight filter. The single output channel per iteration is due to the reasons mentioned above. Instead, further increasing the unrolling factor over the input patches would improve offsets and weights reuse but would lead to a linear increase in the im2col buffer memory overhead. This, in turn, would limit the usability of our kernels for layers with a large number of input channels or big filters, given that the im2col array must necessarily fit in L1.

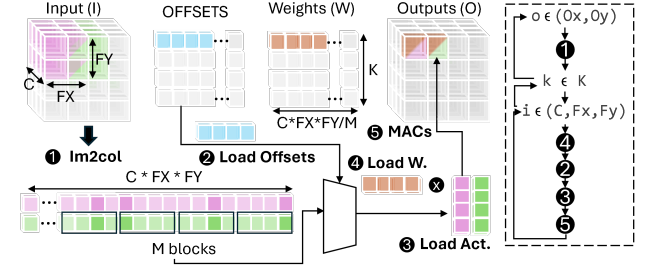


Figure 3. Inner loop of our sparse convolutional kernel.

The key difficulty in implementing kernels for N:M pruning is optimizing the loading of input activations corresponding to NZ weights in the innermost loop. We explored three alternatives:

1) *DMA-based copy*: modify the DMA calls used to move data from L2 to L1 memory to move, for each output channel, only activations corresponding to NZ weights (bypassing the im2col entirely). However, this would eliminate the advantages of DMA burst transfers, leading to highly inefficient loads.

2) *Sparse Im2col*: modify the im2col step to fill the 1-d buffers only with activations corresponding to NZ weights. However, there would be no reuse opportunity for these buffers, as different output channels do not share the NZ indices. The im2col would therefore become a part of the innermost loop, being repeated for every output channel, with a consequent explosion of innermost loop instructions.

3) *Decimate Im2col*: keep the im2col step unchanged while adding a *decimate* step in the innermost loop, that selects only the elements corresponding to NZ weights from the im2col buffer, for each different output channel. Compared to the previous option, the main difference is that the addresses of activations corresponding to NZ weights have to be computed relative to the im2col buffer, and not to the original input tensor. In other words, they are computed as $i \times M + o$, where i identifies the correct block of M elements in the im2col buffer, and o is the relative offset of the NZ weight within the block. Conversely, to load activations directly from the input tensor, we should consider its spatial size (IY, IX) and the center position of each patch to compute the correct address, considering corner cases for different stride and padding combinations, leading to a high number of indexing operations in the innermost loop.

Fig. 3 visualizes our sparse convolutions, which use the latter strategy (*Decimate Im2col*). Fig. 4 (center) details the corresponding innermost loop execution. Here, OFFSETS is the array whose elements store the relative indices of NZ elements in each M-sized block, on 4-bit (for 1:8 and 1:16 sparsity) or 2-bit (for 1:4); the `extractOffset` function uses shift and mask operations to unpack the correct index

DENSE: ARITH. I.: 8/5 = 1.6; MAX. MAC/C.: 1.6	SW SPARSE: ARITH. I.: 8/22=0.36 MAX. MAC/C.: 0.36*M	ISA SPARSE: ARITH. I.: 8/12=0.66. MAX. MAC/C.: 0.66*M
<pre> for(s=0;s<S/2;s++) { // spatial loop, 2x B1, B2 = im2col(X[s]) // im2col step for(k=0;k<K;k++) { // output chs loop for(i=0;i<(C*FX*FY)/4;i++) { // filter loop, 4x vA1=loadW(A1); A1+=4; // Weights load (1) vB1=loadW(B1); B1+=4; // Act. loads (2) vB2=loadW(B2); B2+=4; // - sum1+=dotp(vA1,vB1); // MACs ops (2x4) sum2+=dotp(vA1,vB2); // - } } } </pre>	<pre> for(s=0;s<S/2;s++) { // spatial loop, 2x B1, B2 = im2col(X[s]) // im2col step for(k=0;k<K;k++) { // output chs loop for(i=0;i<(C*FX*FY)/(4*M);i++) { // filter loop, 4Mx vA1=loadW(A1); A1+=4; // Weights load (1) o=loadB(OFFSETS); // Offsets loads (9) pos1=extractOffset(o,0); // - pos2=extractOffset(o,4)+M; // - o=loadB(OFFSETS); // - pos3=extractOffset(o,0)+2*M; // - pos4=extractOffset(o,4)+3*M; // - vB1[0]=loadB(B1+pos1); // Act. loads (8) vB1[1]=loadB(B1+pos2); // - vB1[2]=loadB(B1+pos3); // - vB1[3]=loadB(B1+pos4); // - vB2[0]=loadB(B2+pos1); // - vB2[1]=loadB(B2+pos2); // - vB2[2]=loadB(B2+pos3); // - vB2[3]=loadB(B2+pos4); // - sum1+=dotp(vA1,vB1); // MACs ops (2x4) sum2+=dotp(vA1,vB2); // - B1+=4*M; // Index update (2) B2+=4*M; // - } } } </pre>	<pre> for(int s=0;s<S/2;s++) { // spatial loop, 2x B1, B2 = im2col(X[s]) // im2col step for(int k=0;k<K;k++) { // output chs loop for(int i=0;i<(C*FX*FY)/(4*M);i++) { // filter loop, 4Mx vA1=loadW(A1); A1+=4; // Weights load (1) o=loadW(OFFSETS); // Act. loads (9) xDecimate(vB1, B1, o); // - xDecimate(vB2, B2, o); // - xDecimate(vB1, B1, o); // - xDecimate(vB2, B2, o); // - xDecimate(vB1, B1, o); // - xDecimate(vB2, B2, o); // - xDecimate(vB1, B1, o); // - xDecimate(vB2, B2, o); // - xDecimate(vB1, B1, o); // - xDecimate(vB2, B2, o); // - sum1+=dotp(vA1, vB1, sum1); // MACs ops (2x4) sum2+=dotp(vA1, vB2, sum2); // - } } } </pre>

Figure 4. Innermost iteration of the dense matmul kernel (left), 1:8 / 1:16 sparse kernel with no custom instructions (center), and 1:8 / 1:16 sparse kernel with the `xDecimate` instruction (right).

from each byte-sized element of the array. `vB1` and `vB2`, the two 32-bit registers that store input activations, are filled using the four unpacked indices `pos<i>`. Weights loading and dot products are identical to the dense baseline.

Each iteration of the 1:8 and 1:16 kernels performs 8 MACs and 22 instructions, leading to a peak performance of 0.36 MACs/instructions/core. The 1:4 version has all the four indices required to fill a 32-bit word stored in a single 8-bit `OFFSETS` element, but requires more complex unpacking. Overall, it requires 23 instructions (2 more maskings, one less load) per iteration, leading to a peak of 0.35 MACs/instruction/core. Considering the number of theoretical dense MACs executed, i.e., multiplying the effective number of MACs by the sparsity factor M , we obtain peak performances of 1.4, 2.88, and 5.76 MACs/instruction/core.

4.1.3 ISA-extended Sparse Kernel

The main bottleneck of the SW-based sparse kernels lies in the indices unpacking and vector packing operations; 19 instructions are required to load the two activation registers, `vB1` and `vB2` (9 for computing indices, 8 for loading data, 2 for updating addresses). To tackle this limitation, we design a new instruction, `xDecimate`, to load an 8-bit element from a buffer into a register, given an address and an offset, essentially merging the `extractOffset` function and the load byte operation of the SW-only kernel. Thanks to it, we reduce the instructions to fill the input registers to 8, and the total instructions in the innermost loop from 22 (or 23) to 12, regardless of the sparsity level, as shown in Fig. 4 (right). Thus, we reach a peak of 0.66 MACs/instruction/core, corresponding to 2.64, 5.28, and 10.56 equivalent dense MACs/instruction/core, respectively at 1:4, 1:8 and 1:16 sparsity.

The syntax of the instruction is the following: `xdecimate rd, rs1, rs2`, where `rd` is the register in which ex-

tracted data will be stored, while the two source registers contain the starting address of the `im2col` buffer (`rs1`) and the packed NZ offsets (`rs2`). At a high level, each execution of the instruction loads one activation byte in `rd`, computing the starting address of the target M -sized block in the `im2col` buffer, and adding the correct offset to it. It does so by combining `rs1` and `rs2`, with the value stored in one control-status-registers (`csr1`). The `csr` is auto-incremented at every `xDecimate` operation so that consecutive calls to `xDecimate` automatically point to the correct data. A specific instruction, `xDecimate.clear`, is used to reset it to 0 at the end of the loop over the output channels.

To account for the innermost loop unrolling (over two `im2col` buffers), the M -sized block’s base address and the offset in the destination register are updated only once every two `xDecimate` executions. Instead, the `rs2` bits from which the NZ offset is unpacked are updated every time. This requires *duplicating each NZ index* in the `OFFSETS` array, with a consequent memory overhead. However, it allows us to accommodate, with a single instruction, also the case of FC layers, as detailed in Sec. 4.2.3. Notably, the overhead is acceptable given the low bit-width of indices; we still obtain weight memory savings of 62.5% for 1:4 sparsity, 75% for 1:8, and 87.5% for 1:16. The hardware implementation of `xDecimate` is detailed in Sec. 4.3.

4.2 Fully-Connected Kernel Library

4.2.1 Dense Baseline

The innermost loop of our dense baseline for FC layers (again taken from PULP-NN), is shown in Fig. 5 (left). It is unrolled by a factor of 2 over the K dimension, as FC layers have no opportunities for weight reuse. The efficiency peak

¹We use a lowercase acronym to avoid confusion with CSR, the Compressed Sparse Row format.

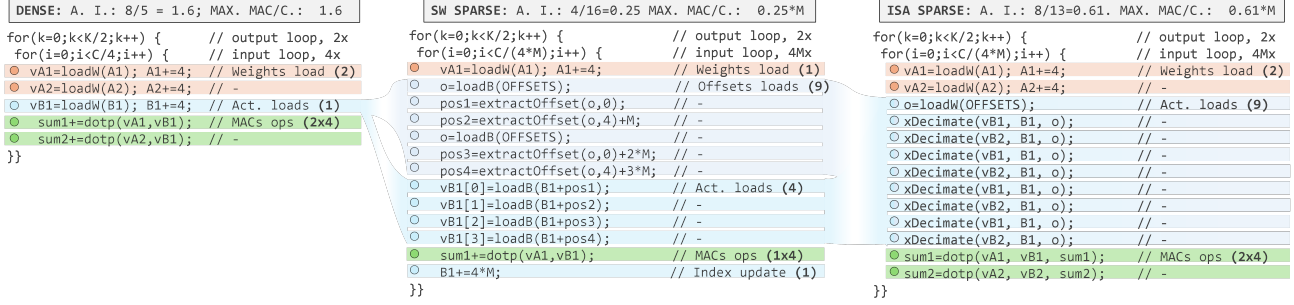


Figure 5. Innermost iteration of the dense FC kernel (left), 1:8 SW-only sparse kernel (center), and 1:8 ISA-extended sparse kernel (right).

for this kernel is 1.6 MACs/instruction/core. Multi-core parallelization is performed on the K dimension.

4.2.2 Software-only Sparse Kernel

We use the same innermost loop as for convolutions, unpacking the indices of four NZ elements and then using them for dot products. The pseudo-code is shown in Fig. 5 (center). Differently from the dense baseline, we do not unroll over two output channels, given that each of them requires different input data. The theoretical peak performance is 0.25 MACs/instruction/core. Considering the equivalent dense MACs, we obtain 1.0, 2.0, and 4.0 MACs/instruction/core for 1:4, 1:8, and 1:16 sparsity. Notice that the 1:4 SW-only sparse kernel does not even reach sufficient theoretical performance to outperform the dense baseline.

4.2.3 ISA-extended Sparse Kernel

The innermost loop of our ISA-extended sparse FC kernel is shown in Fig. 5 (right). To make our HW extension lightweight, we exploit the same `xDecimate` instruction designed for Convolutions. As mentioned in Sec. 4.1.3, the instruction updates the M -sized block’s base address, and the offset in `rd` only once every two executions. For FC layers, which differently from Conv are not unrolled over two `im2col` buffers, we do not duplicate the NZ offsets, but rather, we reorganize them (offline). Namely, we construct the `OFFSETS` array by alternating the offsets of NZ elements in two consecutive channels (i.e., o_{0,ch_i} , $o_{0,ch_{i+1}}$, o_{1,ch_i} , $o_{1,ch_{i+1}}$, etc.). In the kernel’s inner loop, we load NZ weights for channels i and $i+1$ in two 4x8-bit registers (`vA1` and `vA2`), before calling `xDecimate` eight times to load 8 activations from a single `im2col` buffer, alternating `vB1` and `vB2` as destinations. As a result, `vB1` will eventually contain the activations corresponding to the i -th channel’s NZ weights, and `vB2` those corresponding to the $i+1$ -th channel, allowing to perform 8 MACs. In other words, we essentially unroll over two output channels ($K = 2$) despite not having input reuse opportunities, with the objective of maintaining the same exact instruction originally designed for Convolutions. Fig. 6 shows the complete flow. The theoretical peak performance obtained with this kernel is

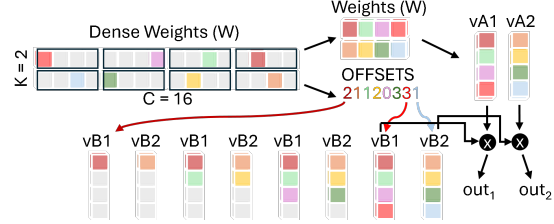


Figure 6. For FC layers, NZ OFFSETS are reorganized offline alternating 2 output channels. Activations are then loaded in two buffers `vB1` and `vB2` (example for 1:4 sparsity).

0.61 dense equivalent MACs/instruction/core, which translates to 2.44, 4.88, and 9.76 MACs/instruction/core, always outperforming the dense baseline.

4.3 xDecimate Hardware Implementation

We prototyped the functionality of the `xDecimate` instruction at the register-transfer level (RTL) inside the open-source RISCY/CV32E40P processor² used in (Rossi et al., 2021). RISCY implements the RV32IMC ISA with the addition of the `Xpulpv2` extension, which includes hardware loops, load/store with post-increment, SIMD dot-product instructions, etc. We modified the processor adding an extension Functional Unit (XFU), whose microarchitecture is shown in Fig. 7, which encompasses three of the four stages of RISCY’s pipeline: Instruction Decode (ID), Execute (EX), and Write-Back (WB). Differently from regular RISC-V loads, the `xDecimate` instruction employs an R-type encoding with two source registers `rs1`, `rs2` and one destination register `rd`; all three registers are simultaneously read from the register file (RF, not shown in Fig. 7) in the ID stage, exploiting RISCY’s 3-read port RF, which is also necessary for the `Xpulpv2` extension. A lightweight decoder identifies which flavor of `xDecimate` (i.e., which sparsity format) is being used.

The EX stage implements the extension’s main functionality,

²<https://github.com/openhwgroup/cv32e40p>

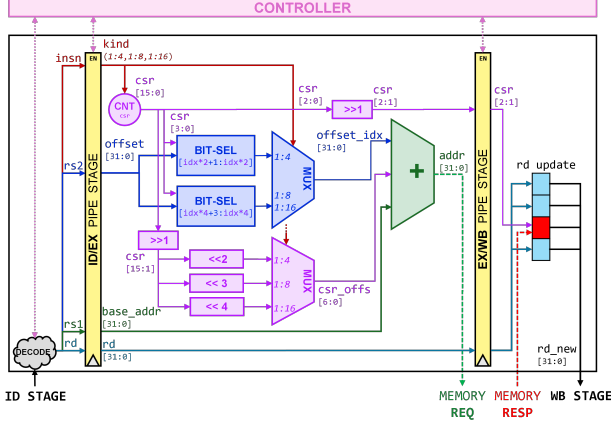


Figure 7. Detail of xDecimate eXtension Functional Unit (XFU) micro-architecture prototyped inside the RI5CY processor.

which for 1:8 and 1:16 sparsity, can be summarized as:

$$\begin{aligned} o &\leftarrow rs2[(csr[2:0] * 4 + 3) : (csr[2:0] * 4)] \\ addr &\leftarrow rs1 + M * csr[15:1] + o \end{aligned}$$

The `csr` is used to select the appropriate bits to unpack the NZ offset from the 32-bit word loaded in `rs2`. The `csr` is also used to compute the starting address of the current M-sized block. For this, it is right-shifted by one position, thus ensuring that two consecutive xDecimate calls point to the same block (thus accounting for our inner loop unrolling). Both offsets are added to the base address loaded in `rs1`, and the result is propagated as a memory request through RI5CY’s load/store unit. The instruction for 1:4 sparsity is similar, just using 4 `csr` LSBs instead of 3, given that `rs2` contains 16 2-bit wide offsets in this case.

In the WB stage, the interesting byte is extracted from the memory response and written into the `rd` register in the position selected by the `csr` (again right-shifted to account for unrolling). The updated `rd` is propagated back to RI5CY’s RF. Then, the `csr` is automatically incremented to prepare for the next execution. Formally:

$$\begin{aligned} rd[(csr[2:1] * 8 + 7) : (csr[2:1] * 8)] &\leftarrow MEM[addr] \\ csr &\leftarrow csr + 1 \end{aligned}$$

The XFU controller also checks for data dependencies between consecutive xDecimate instructions to enable forwarding the value of `rd` from the WB stage.

4.4 Integration in the MATCH Compiler

To run end-to-end neural networks and support layer tiling, we integrate our sparse kernels into MATCH (Hamdi et al., 2024), an extension to Apache TVM for heterogeneous

SoCs. We added three main features to MATCH to support our sparse kernels efficiently:

1) Modified Pattern Recognition: the first compilation step of MATCH associates DNN graph patterns to known acceleration targets based on a HW-specific pattern table. Starting from the existing PULP target, we added new patterns that extend the ones already present for convolutional/FC layers, with an additional constraint on the weights’ values, checking the NZ weights positions and recognizing 1:4, 1:8, or 1:16 sparsity formats.

2) Tiling for Sparse Kernels: the integration of N:M sparse kernels requires tiling both the NZ weight tensors and the associated NZ indices. Our modified tiling engine optimizes the tile layout by taking into account both the reduced dimension of the weights and the overhead due to the indices. To do so, we simply changed the number of bits associated with each weight. As an example, considering 1:4 sparsity, we need 12 bits to store each NZ weight (8 bits for the value, 4 bits for the replicated weight offset). Since the other 3 weights are zero, this is equivalent to having 3-bit per dense-equivalent weight. Thanks to this modification to the tiling engine, we are able to tile sparse layers better, obtaining additional speed-ups due to better L1 utilization.

3) Weights Memory Storage: To further enhance performance, we modify the memory layout handling in MATCH to better support the simultaneous transfer of the compressed weights and their corresponding indices. In our approach, the weights and indices are stored in L2 memory in an interleaved fashion. Specifically, if a layer is tiled on $K/2$ output channels, MATCH stores the corresponding half of the weights, followed by the corresponding indices, so that both can be transferred with a single DMA transaction. Once the first tile has been processed, the second half of weights and indices are fetched in the same manner.

5 RESULTS

5.1 Experimental Setup

We benchmark our proposed kernels and two end-to-end networks using the GVSoC virtual platform (Bruschi et al., 2021) to simulate Vega (Rossi et al., 2021). The HW extension has been implemented in SystemVerilog RTL and synthesized using Synopsys Design Compiler targeting the same 22nm technology as (Rossi et al., 2021) with 200 MHz target clock frequency in worst-case operating conditions (slow-slow process, 0.72 V operating voltage, 125 C temperature). The two DNNs are a ResNet18 (He et al., 2016), trained on Cifar100, and a Vision Transformer (Dosovitskiy et al., 2020) (ViT-Small), trained on a rescaled 224x224 version of Cifar10. Both have been trained for 200 epochs using the combined training and pruning scheme detailed in (Zhou et al., 2021). For ResNet, we apply N:M pruning

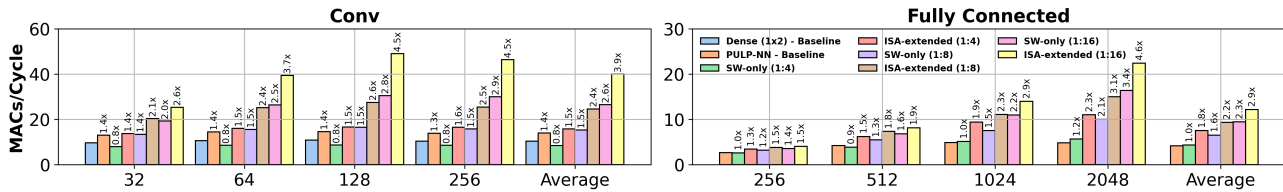


Figure 8. Single-layer results. Bars are grouped by input channels/features (C). Numbers report speedups over the dense 1x2 baseline.

to 3x3 convolutions, leaving pointwise layers dense. For the ViT, we sparsify only the FC layers of the feed-forward block. After training, we quantize all networks to 8 bits using Brevitas (Pappalardo, 2023). All individual kernels and end-to-end ResNets have been deployed using the modified MATCH compiler. For ViTs, given the lack of support for attention layers in MATCH, we computed the latency layer-by-layer, using Deeploy (Scherer et al., 2024), an alternative compiler for the same HW, for attention layers, and MATCH for sparse/dense feed-forward layers. The reported MACs/cycle values always refer to dense-equivalent operations.

5.2 Single Layers Benchmarking

We first benchmark both convolutional and FC layers, varying the input channels/neurons dimension while keeping other parameters fixed; we set the output channels/neurons $K = 256$, and for convolutions, we also use $IX/IY = OX/OY = 8$, $FX/FY = 3$, $S = 1$, $P = 1$. We vary $C \in [32, 64, 128, 256]$ for convolutions and $C \in [256, 512, 1024, 2048]$ for FC layers. Fig. 8 shows the performance of 1:4, 1:8, and 1:16 sparse kernels, without (SW) our with (ISA) \times Decimate, as well as the results of the two dense baselines, 1x2 and PULP-NN (FC layers have a single baseline, given that also PULP-NN uses 1x2 unrolling).

As expected from the inner loop instructions analysis of Sec. 4 the 1:4 SW-only Convolution performs worse than the dense versions (+23% cycles on average, w.r.t. the 1x2 baseline). At the other extreme, the 1:16 SW-only kernel obtains an average speedup of 2.6 \times and 1.85 \times compared to the 1x2 and the PULP-NN baselines. Notice that the lower speed-up compared to the theoretical one obtained comparing inner loop instructions (3.6 \times vs the 1x2 baseline) is mainly due to the im2col step, which is identical in sparse and dense kernels and reduces the overall MACs/cycle performance. ISA-extended kernels further improve performance, making 1:4 sparsity advantageous too, with an average speedup of 1.50 \times and 1.12 \times over 1x2 and PULP-NN. At 1:8 sparsity, the speedups grow to 2.4 \times and 1.74 \times , and at 1:16 sparsity, to 3.9 \times and 2.78 \times , respectively. For all kernels, performance tends to improve with increasing C; the improvement is more marked for sparser layers, given that our kernels accelerate the innermost matrix multiplication loop, whose relative importance over the constant im2col phase grows

with C. At $C=256$, given the high occupation of the im2col buffer, L1 tiles for Conv layers over spatial dimensions start to be very small. Thus, performance reduces slightly.

For FC layers, SW-only sparse kernels outperform the baselines even at 1:4 sparsity, albeit with modest latency reductions (2% on average). This is particularly evident on larger geometries (e.g., $C = 2048$), where the speedup reaches 1.2 \times . Although there is no theoretical gain in the inner loop, this improvement derives from the fewer weight loads required, given the lower memory footprint of sparse weights. This contribution is less evident (or absent) for convolutions, where the latency of weights transfers from L2 to L1 is hidden using double-buffering (Hamdi et al., 2024). For memory-bound FC layers, instead, these transfers are one of the dominant components of the overall latency. At higher sparsity ratios (1:8 and 1:16), the average speedups increase to 1.6 \times and 2.3 \times , respectively, with peaks up to 3.4 \times . ISA-extended kernels yield more significant improvements, achieving an average 1.8 \times speedup at 1:4 sparsity with a peak of 2.3 \times for $C = 2048$. At 1:8 and 1:16 sparsity, the average speedups are 2.2 \times and 2.9 \times , respectively.

5.3 End-to-end DNNs Benchmarking

Table 2 reports profiling results of end-to-end models. We also report the accuracy obtained by our sparse models to demonstrate that the considered sparsity patterns are applicable to real-world applications, leading in most cases to null or small degradations.

In the ViT model, the sparsified FC layers account for 65% of the model’s parameters and 60% of the operations. Despite the relevant parameters reduction, even with the most aggressive pruning pattern (1:16), sparsifying these layers impacts the accuracy minimally, with a drop of 0.42%. On the other hand, in terms of latency, all sparsified models, both with and without the new \times Decimate operation, outperform the dense baseline. Using SW-only kernels, we achieve speedups of 1.03 \times , 1.36 \times , and 1.63 \times , respectively, at 1:4, 1:8, and 1:16 sparsity. ISA-extended kernels outperform the dense models even further, achieving speedups of 1.43 \times , 1.61 \times , and 1.81 \times . Overall, our most compressed model (1:16) achieves 95.17% accuracy with a 2.34 \times lower memory footprint compared to the dense counterpart and a 1.81 \times latency reduction when using our ISA extension.

Table 2. End-to-end models results on the (Rossi et al., 2021) platform.

Model	Dataset	Sparsity	Acc.[%]	SW-only kernels			ISA-extended kernels		
				MAC/cyc.	Cyc.[M]	Mem.[MB]	MAC/cyc.	Cyc.[M]	Mem.[MB]
ViT	CIFAR10	Dense	95.59	4.65	975.23	21.59	-	-	-
		1:4	95.73	4.80	944.17	11.86	6.66	681.19	11.86
		1:8	95.02	6.31	718.86	10.09	7.48	606.99	10.09
		1:16	95.17	7.59	598.04	8.76	8.40	540.23	8.76
ResNet18	CIFAR100	Dense 1x2	75.28	8.33	66.63	11.22	-	-	-
		PULP-NN	75.28	11.17	49.71	11.22	-	-	-
		1:4	75.78	8.11	68.44	3.66	14.74	37.67	4.35
		1:8	75.63	14.78	37.57	2.29	23.12	24.01	2.98
		1:16	73.79	25.85	21.48	1.26	35.87	15.48	1.6

Concerning ResNet18, the sparsified convolutions (all but the pointwise) account for 97% of the total parameters and 98% of the total MACs. Training the models with 1:4 and 1:8 sparsity, we obtained even higher accuracy than the dense network, while 1:16 yields a slight performance drop of 1.49%. In terms of latency, similarly to the result obtained on single layers, the model that leverages the 1:4 SW-only kernels is outperformed by both dense baselines (1x2 and PULP-NN), achieving 1.03x and 1.38x higher latency, although it reduces the memory footprint from 11.22 MB to 3.66 MB. SW-only sparse models outperform their dense counterparts at 1:8 and 1:16 sparsity. With the ISA extension, all sparse ResNets achieve speedups against both baselines. The most compressed model that does not incur accuracy drops uses 1:8 sparsity, reaching 0.35% higher accuracy, 2.07x lower latency, and 3.77x lower memory footprint compared to the best dense option, i.e., PULP-NN. Notice that ResNet versions using xDecimate require slightly more memory than SW-only ones due to the replication of NZ indices in Conv kernels (see Sec. 4.1.3).

5.4 SoTA Comparison

Table 3 compares our work with the SotA on sparse acceleration for MCUs. We report the benchmark DNNs, the sparsity level, the speedup obtained w.r.t. a dense execution, and the area overhead, if present. Concerning our results, we report those on ResNet since, to our knowledge, no SotA work considered N:M pruning for transformers on MCUs.

The authors of (Yu et al., 2017) report speedups from 1.31x to 9.17x. At a high sparsity ($\geq 90\%$), they achieve 3.21x speed-up over a dense LeNet CNN and 9.17x on the FC-only LeNet300. As anticipated in Sec. 3, the high speed-up on the LeNet300 is caused by the high-latency loads from Flash memory. Since FC models are memory-bound, strongly reducing the number of loads almost linearly translates to latency savings. Conversely, on more compute-bound CNNs, the load latency impact is lower, and our ISA-extended solution achieves better speed-ups for both aggressive (4.31x vs 3.51x at $\geq 90\%$ sparsity) and moderate pruning (1.77x vs 1.38x for 75% vs 59.9% sparsity).

Table 3. Comparison with the state-of-the-art.

Benchmark	Spars.	Speedup	Area[%]
LeNet ¹	93.28%	3.51	-
ConvNet ¹	59.9%	1.38	-
LeNet300 ¹	93.07%	9.17	-
DS-CNN ²	90%	1.71	-
ResNet50 ³	75%	1.82*	n.a.
DenseNet ³	75%	2.14*	n.a.
InceptionV3 ³	75%	1.92*	n.a.
spMV ⁴	95.7%	5*	44
ResNet18-SW	87.5-93.75%	1.77-3.10	-
ResNet18-ISA	75-93.75%	1.77-4.31	5

¹ (Yu et al., 2017), ² (Trommer et al., 2021), ³ (Titopoulos et al., 2023), ⁴ (Scheffler et al., 2023), * speedup compared to SW-only sparse baseline

With SW-only kernels, we achieve comparable results.

The Large DS-CNN from (Trommer et al., 2021), at 90% sparsity, achieves 1.71x speed-up compared to dense unoptimized CMSIS-NN kernels. Similarly, at 87.5% sparsity, we obtain 1.77x/2.77x speed-ups with the SW and ISA kernels compared to the 1x2 baseline. Note also that, with the N:M format, we obtain a memory reduction of 79.59/73.44%, compared to the 74.45% obtained by (Trommer et al., 2021), with similar levels of sparsity (87.5% vs 90%).

In (Titopoulos et al., 2023), the authors report speedups of 1.82/1.92/2.14x on different convolutional networks at 75% sparsity, comparing their ISA-enhanced results to SW-only sparse kernels. On our ResNet18 model at iso-sparsity, thanks to xDecimate, we achieve a 1.82x speedup w.r.t. the SW-only version, despite the fact that our HW extension, being tailored for ultra-low-power edge devices, is much more lightweight than the one in (Titopoulos et al., 2023), which leverages a large vector RF on a more powerful core (and whose area overhead is not reported).

In (Scheffler et al., 2023), a 5x speedup over SW-only sparse kernels for GEMM is reported, at 95.7% sparsity, higher than the 1.39x@93.75% sparsity (i.e. 1:16) that we achieve with our ISA extension vs the SW-only ResNet18. However, note that for such extreme values a sparsity, an

apparently small difference corresponds to executing 6.25% of the original MACs (in our case), vs 4.3% (i.e. $1.45\times$ fewer) in (Scheffler et al., 2023). Furthermore, the HW support required to achieve such an acceleration leads to an area overhead of 44% w.r.t. an FPU-less core like ours, versus our 5%.

6 CONCLUSIONS

We have introduced a set of efficient kernels N:M pruning on MCUs of the PULP family, and a lightweight extension of the XPulpV2 ISA, to further speed them up. On the platform described in (Rossi et al., 2021), and targeting a ViT and a ResNet18, we have achieved end-to-end latency reductions of $1.81\times$ and $3.21\times$, with less than 0.5/1.5% accuracy drop on CIFAR10/CIFAR100 respectively.

REFERENCES

- Bruschi, N., Haugou, G., Tagliavini, G., Conti, F., Benini, L., and Rossi, D. GVSoc: A Highly Configurable, Fast and Accurate Full-Platform Simulator for RISC-V based IoT Processors. In *2021 IEEE 39th International Conference on Computer Design (ICCD)*, pp. 409–416, 2021.
- Castro, R. L., Ivanov, A., Andrade, D., Ben-Nun, T., Fraguera, B. B., and Hoefler, T. VENOM: A Vectorized N:M Format for Unleashing the Power of Sparse Tensor Cores. In *Proceedings of the International Conference for High Performance Computing, Networking, Storage and Analysis, SC '23*, New York, NY, USA, 2023. Association for Computing Machinery. ISBN 9798400701092.
- Chen, Y.-H., Yang, T.-J., Emer, J., and Sze, V. Eyeriss v2: A flexible accelerator for emerging deep neural networks on mobile devices. *IEEE Journal on Emerging and Selected Topics in Circuits and Systems*, 9(2):292–308, 2019.
- Devlin, J., Chang, M.-W., Lee, K., and Toutanova, K. Bert: Pre-training of deep bidirectional transformers for language understanding. In *Proceedings of the 2019 conference of the North American chapter of the association for computational linguistics: human language technologies, volume 1 (long and short papers)*, pp. 4171–4186, 2019.
- Dosovitskiy, A., Beyer, L., Kolesnikov, A., Weissenborn, D., Zhai, X., Unterthiner, T., Dehghani, M., Minderer, M., Heigold, G., Gelly, S., et al. An image is worth 16×16 words: Transformers for image recognition at scale. *arXiv preprint arXiv:2010.11929*, 2020.
- Garofalo, A., Rusci, M., Conti, F., Rossi, D., and Benini, L. PULP-NN: Accelerating quantized neural networks on parallel ultra-low-power RISC-V processors. *Philosophical Transactions of the Royal Society A*, 378(2164): 20190155, 2020.
- Gautschi, M., Schiavone, P. D., Traber, A., Loi, I., Pullini, A., Rossi, D., Flamand, E., Gürkaynak, F. K., and Benini, L. Near-Threshold RISC-V Core With DSP Extensions for Scalable IoT Endpoint Devices. *IEEE Trans. Very Large Scale Integr. Syst.*, 25(10):2700–2713, October 2017. ISSN 1063-8210.
- GreenWaves. GAP9. https://greenwaves-technologies.com/gap9_processor/, 2024. [Accessed 10-06-2024].
- Guo, C., Hsueh, B. Y., Leng, J., Qiu, Y., Guan, Y., Wang, Z., Jia, X., Li, X., Guo, M., and Zhu, Y. Accelerating sparse DNN models without hardware-support via tile-wise sparsity. In *SC20: International Conference for High Performance Computing, Networking, Storage and Analysis*, pp. 1–15. IEEE, 2020.
- Hamdi, M. A., Daghero, F., Sarda, G. M., Van Delm, J., Symons, A., Benini, L., Verhelst, M., Pagliari, D. J., and Burrello, A. MATCH: Model-Aware TVM-based Compilation for Heterogeneous Edge Devices. *arXiv preprint arXiv:2410.08855*, 2024.
- Han, S., Liu, X., Mao, H., Pu, J., Pedram, A., Horowitz, M. A., and Dally, W. J. EIE: Efficient Inference Engine on Compressed Deep Neural Network. In *2016 ACM/IEEE 43rd Annual International Symposium on Computer Architecture (ISCA)*, pp. 243–254, 2016.
- He, K., Zhang, X., Ren, S., and Sun, J. Deep residual learning for image recognition. In *Proceedings of the IEEE conference on computer vision and pattern recognition*, pp. 770–778, 2016.
- Hoefler, T., Alistarh, D., Ben-Nun, T., Dryden, N., and Peste, A. Sparsity in deep learning: Pruning and growth for efficient inference and training in neural networks. *Journal of Machine Learning Research*, 22(241):1–124, 2021.
- Jeong, G., Damani, S., Bambhaniya, A. R., Qin, E., Hughes, C. J., Subramoney, S., Kim, H., and Krishna, T. VEG-ETA: Vertically-Integrated Extensions for Sparse/Dense GEMM Tile Acceleration on CPUs. In *2023 IEEE International Symposium on High-Performance Computer Architecture (HPCA)*, pp. 259–272. IEEE, 2023.
- Lai, L., Suda, N., and Chandra, V. CMSIS-NN: Efficient neural network kernels for Arm Cortex-M CPUs. *arXiv preprint arXiv:1801.06601*, 2018.
- Li, G., Ma, X., Wang, X., Yue, H., Li, J., Liu, L., Feng, X., and Xue, J. Optimizing deep neural networks on intelligent edge accelerators via flexible-rate filter pruning. *Journal of Systems Architecture*, 124:102431, 2022a.

- Li, S., Osawa, K., and Hoefler, T. Efficient quantized sparse matrix operations on tensor cores. In *SC22: International Conference for High Performance Computing, Networking, Storage and Analysis*, pp. 1–15. IEEE, 2022b.
- Ma, X., Fang, G., and Wang, X. LLM-Pruner: On the structural pruning of large language models. *Advances in neural information processing systems*, 36:21702–21720, 2023.
- Nagel, M., Fournarakis, M., Amjad, R. A., Bondarenko, Y., Van Baalen, M., and Blankevoort, T. A white paper on neural network quantization. *arXiv preprint arXiv:2106.08295*, 2021.
- NVIDIA. A100 tensor core gpu architecture. <https://images.nvidia.com/aem-dam/en-zz/Solutions/data-center/nvidia-ampere-architecture-whitepaper.pdf>, 2020. [Accessed 10-06-2024].
- NVIDIA. TensorRT. <https://developer.nvidia.com/tensorrt/>, 2024. [Accessed 10-06-2024].
- NXP. LPC4300. https://www.nxp.com/products/processors-and-microcontrollers/arm-microcontrollers/general-purpose-mcus/lpc4300-arm-cortex-m4-m0:MC_1403790133078#/, 2024. [Accessed 10-06-2024].
- Pappalardo, A. Xilinx/brevitas, 2023. URL <https://doi.org/10.5281/zenodo.3333552>.
- Park, J., Li, S., Wen, W., Tang, P. T. P., Li, H., Chen, Y., and Dubey, P. Faster cnns with direct sparse convolutions and guided pruning. *arXiv preprint arXiv:1608.01409*, 2016.
- Peltekis, C., Titopoulos, V., Nicopoulos, C., and Dimitrakopoulos, G. DeMM: A Decoupled Matrix Multiplication Engine Supporting Relaxed Structured Sparsity. *IEEE Computer Architecture Letters*, 23(1):17–20, 2024.
- Raffel, C., Shazeer, N., Roberts, A., Lee, K., Narang, S., Matena, M., Zhou, Y., Li, W., and Liu, P. J. Exploring the limits of transfer learning with a unified text-to-text transformer. *Journal of machine learning research*, 21(140):1–67, 2020.
- Rossi, D., Conti, F., Eggiman, M., Di Mauro, A., Tagliavini, G., Mach, S., Guermandi, M., Pullini, A., Loi, I., Chen, J., et al. Vega: A ten-core SoC for IoT endnodes with DNN acceleration and cognitive wake-up from MRAM-based state-retentive sleep mode. *IEEE Journal of Solid-State Circuits*, 57(1):127–139, 2021.
- Scheffler, P., Zaruba, F., Schuiki, F., Hoefler, T., and Benini, L. Sparse Stream Semantic Registers: A Lightweight ISA Extension Accelerating General Sparse Linear Algebra. *IEEE Transactions on Parallel and Distributed Systems*, 2023.
- Scherer, M., Macan, L., Jung, V., Wiese, P., Bompani, L., Burrello, A., Conti, F., and Benini, L. Deeploy: Enabling Energy-Efficient Deployment of Small Language Models On Heterogeneous Microcontrollers. *arXiv preprint arXiv:2408.04413*, 2024.
- Schuiki, F., Zaruba, F., Hoefler, T., and Benini, L. Stream semantic registers: A lightweight RISC-V ISA extension achieving full compute utilization in single-issue cores. *IEEE Transactions on Computers*, 70(2):212–227, 2020.
- Shi, W., Cao, J., Zhang, Q., Li, Y., and Xu, L. Edge computing: Vision and challenges. *IEEE internet of things journal*, 3(5):637–646, 2016.
- STMicroelectronics. STM32H7. <https://www.st.com/en/microcontrollers-microprocessors/stm32h7-series.html>, 2024. [Accessed 10-06-2024].
- Sze, V., Chen, Y.-H., Yang, T.-J., and Emer, J. S. Efficient processing of deep neural networks: A tutorial and survey. *Proceedings of the IEEE*, 105(12):2295–2329, 2017.
- Tan, Y., Han, K., Zhao, K., Yu, X., Du, Z., Chen, Y., Wang, Y., and Yao, J. Accelerating Sparse Convolution with Column Vector-Wise Sparsity. In Koyejo, S., Mohamed, S., Agarwal, A., Belgrave, D., Cho, K., and Oh, A. (eds.), *Advances in Neural Information Processing Systems*, volume 35, pp. 30307–30317. Curran Associates, Inc., 2022.
- Titopoulos, V., Alexandridis, K., Peltekis, C., Nicopoulos, C., and Dimitrakopoulos, G. Indexmac: A custom risc-v vector instruction to accelerate structured-sparse matrix multiplications. *arXiv preprint arXiv:2311.07241*, 2023.
- Trommer, E., Waschneck, B., and Kumar, A. dcsr: a memory-efficient sparse matrix representation for parallel neural network inference. In *2021 IEEE/ACM International Conference On Computer Aided Design (ICCAD)*, pp. 1–9. IEEE, 2021.
- Wang, F., Zhang, M., Wang, X., Ma, X., and Liu, J. Deep learning for edge computing applications: A state-of-the-art survey. *IEEE Access*, 8:58322–58336, 2020.
- Wang, Z. SparseDNN: Fast sparse deep learning inference on CPUs. *arXiv preprint arXiv:2101.07948*, 2021.

- Wu, B., Dai, X., Zhang, P., Wang, Y., Sun, F., Wu, Y., Tian, Y., Vajda, P., Jia, Y., and Keutzer, K. FBNet: Hardware-Aware Efficient ConvNet Design via Differentiable Neural Architecture Search. In *Proceedings of the IEEE/CVF conference on computer vision and pattern recognition*, pp. 10734–10742, 2019.
- Wu, H., Judd, P., Zhang, X., Isaev, M., and Micikevicius, P. Integer quantization for deep learning inference: Principles and empirical evaluation. *arXiv preprint arXiv:2004.09602*, 2020.
- Yu, J., Lukefahr, A., Palframan, D., Dasika, G., Das, R., and Mahlke, S. Scalpel: Customizing DNN pruning to the underlying hardware parallelism. *ACM SIGARCH Computer Architecture News*, 45(2):548–560, 2017.
- Zhou, A., Ma, Y., Zhu, J., Liu, J., Zhang, Z., Yuan, K., Sun, W., and Li, H. Learning N: M Fine-grained Structured Sparse Neural Networks From Scratch. *arXiv preprint arXiv:2102.04010*, 2021.